Journal of Applied Polymer Science

Characterization of Silica/PET Antiglare Films Using Image Analysis and Dynamic Dispersity Index

In Hwan Sul,[1] Young Seok Song[2]

[1]Korean Intellectual Property Office, Room 905, 4-Dong, Government Complex-Daejeon, Daejeon, Republic of Korea
[2]Department of Fiber System Engineering, Dankook University, 126 Jukjeon-dong, Suji-gu, Yongin-si, Gyeonggi-do, Republic of Korea
Correspondence to: Y. S. Song (E-mail: ysong@dankook.ac.kr)

ABSTRACT: This article proposes an advanced theoretical framework that quantitatively evaluates dispersion state of silica beads of a PET-based antiglare film. The positional randomness of bead dispersion is expressed via a single scalar value, the dynamic dispersity index. The static dispersity index definition based on molecular dynamics, which was proposed in our previous work, was improved with a pseudo-relaxation algorithm. PET-based antiglare films, which had the variable degree of particle dispersion, were used for the verification together with graphically drawn artificial bead images. © 2013 Wiley Periodicals, Inc. J. Appl. Polym. Sci. 129: 3518–3526, 2013

KEYWORDS: colloids; light scattering; optical and photovoltaic applications

Received 2 January 2013; accepted 31 January 2013; published online 28 February 2013
DOI: 10.1002/app.39116

INTRODUCTION

In the field of flat panel displays such as liquid crystal displays, plasma displays, and electro-luminescent displays, an antiglare (AG) film having a concave–convex structure on the surface, or an antireflectance film, is provided on the display surface in order to prevent the decrease of visibility caused by reflection of an external light on the display surface during viewing.[1,2] Such a concave–convex structure, generally formed by silica particles on a polyethylene terephthalate (PET),[3,4] TAC,[4–7] or PVA[7,8] substrate, enhances the value of the display by preventing the specular reflection of lights.

This paper is an initiative step for series of researches aimed at objective evaluation of AG properties of AG films. It is our long-term and final project to assess the degree of AG property both precisely and objectively. As a first step, this paper finds a way to produce a constant level of AG films, i.e., our primary concern is to pursue quality control in an AG film manufacturing process. Thus, we need an objective and an efficient tool to evaluate the quality of AG films.

First of all, it is necessary to define the concept of AG film quality. A good AG film needs to fulfill several conditions such as haze, gloss, flame resistance, antistatic property, scratch resistance, and so on.[3,4,9,10] The most important factor of them is the AG property with no doubt. Nonetheless, it is not easy to find a direct measurement method for the evaluation of the AG films' AG property and indirect methods such as haze and gloss measurements have been used as alternatives. Generally, the haze means cloudiness of a film that is caused by the light scattering. In other words, the higher haze value means the more opaque film. Meanwhile, the gloss is a ratio of specular light reflection to a certain incident angle. The haze of 1–15 and the gloss of 60–100% is said to be a suitable level for good AG property.[11] Both methods are more objective than visual assessment, because their measurement mechanism is based on reflection of light. But they cannot represent the quality of the AG film, which is defined as a dispersity of beads herein, directly. This is because their results are statistical averages over a relative wide area, e.g., over at least 1 mm^2. Also no obvious relationship has been established between the bead dispersity and the light reflection yet. Therefore, the haze and gloss values are not suitable candidates for the direct measurement of the bead dispersity.

The other methodology for the indirect measurement of the bead dispersity is profiling a surface roughness. *Z*-coordinates of a specimen surface are acquired using a metallic stylus, similarly to the mechanism of atomic force microscopy.[12,13] Statistical values such as average and standard deviation of surface height data are used as the indices for the surface roughness. Advantages of this method include cheap equipment and easy experiment procedure. This method differs from the atomic force microscopy in that it scans the specimen only in a linear path, not over the whole two-dimensional specimen area. Thus it cannot represent the general tendency of the bead dispersity either.

The more desirable way of measuring the bead dispersity may be to use information of bead positions. Such a idea was already proposed by several researchers. Liu[14] divided the raw specimen image into rows and columns of small rectangular blocks and counted the number of beads inside each block. Also Diebold[15] assigned relatively many reference points over the raw image and counted the number of beads inside a certain distance from each reference point. Both methods gave the less standard deviation value for the better-distributed beads. But they needed a sufficiently large number of beads, blocks, or reference points to yield a meaningful result. And they were not tolerant of even slight changes of threshold values. These statistics-based methods did not give a reliable result for the AG films where the number of beads is not more than 1000. A point of excellence in their methods will be that they are nondestructive and the calculation results are more statistically general than the surface roughness test because the whole 2-D specimen area is taken into account.

Table I. Test Results for Four Specimens

ID	Haze (internal)	Gloss (60°/45°/20°)	Roughness		
			Ra	Rz	Sm
L1	8.6	44/88/90	0.0864	0.8506	29.4
F1	6.6	47/95/93	0.0712	0.7775	26.6
F2	6.4	59/105/96	0.0475	0.5645	23.1
F3	7.2	44/92/93	0.0662	0.6672	23.0

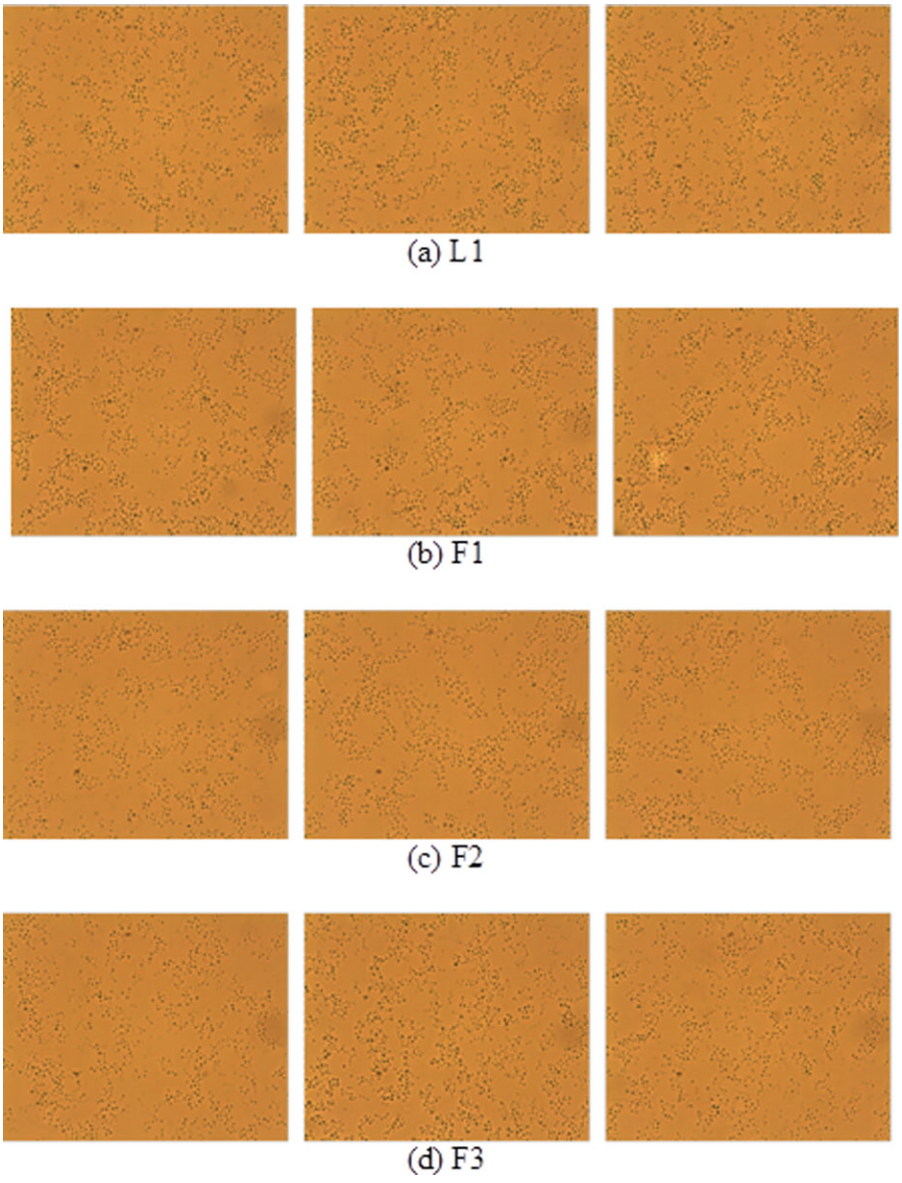

Figure 1. Microscopic images of specimens (×500 magnification). [Color figure can be viewed in the online issue, which is available at wileyonlinelibrary.com.]

Huckaby and Cairns[16] also adopted the image analysis to quantify the reflection amount of laser on AG-textured surfaces. They used three different types of AG surfaces for specimens, such as an acid-etched surface, a sol-gel sprayed surface, and a nano-particle roughened surface. The gloss value with an incident ray angle of 60° and the final reflected laser intensity was measured as an indirect index of surface sparkling. Speckle contrast may be somewhat related with the bead dispersion state, but it is also a statistical average of the light reflectance area. And it cannot be a direct barometer for the bead dispersity.

This article proposes an advanced evaluation method of the dispersity index of the AG film beads for flat panel displays, which is a nondestructive, instant and direct representation of the dispersion state. Bead positions were detected automatically from a microscopic image using image analysis techniques, and their relative movement to form a hexagonal packing was simulated. The inter-particle interaction was measured using potentials based on molecular dynamics, which is modified from our previous work,[17] and the total interaction energy dissipated during the relaxation was defined as a new dispersity index, i.e., dynamic dispersity index. The new method was verified by comparing the graphically drawn bead image sets and the real haze test results of the AG films. Experimental and theoretical details will be dealt in materials and testing equipments sections, respectively, followed by results and discussion section.

MATERIALS

A hard coat material including silica particles and base films was prepared for the evaluation test. Other inner layers including a PVA-based polarization layer and a TAC-based protection layer were omitted.

An ultraviolet-curing resin (DAINICHI SEIKA KOGYO, SEIKABEAM EXF-01J, a polyester acrylate), a dispersion of colloidal silica particles in isopropyl alcohol (SHOKUBAI KASEI KOGYO, OSCAL1432, average particle diameter: 10–20 nm) and 1,8-azabicyclo[5.4.0]undeca-7-ene (KANTO KAGAKU) were mixed. To the obtained mixture, isopropyl alcohol, ethylcellulose, and methyl ethyl ketone were added and mixed well to prepare a hard coat material. The agglomerates of the colloidal silica particles formed with the amine had an average diameter of about 3μm.

Then, a film of PET having a thickness of 125 μm (TORAY; LUMILAR T60) was coated with the above-stated hard coat material in such an amount that the cured hard coat layer had a thickness of 4 μm, and the obtained product was dried at 80°C for 1 min. The dried layer was irradiated with ultraviolet light radiation device (AI GRAPHICS; UB042-5AM-W) in an amount of 300 mJ/cm^2 to prepare a hard coat film by curing.

TESTING EQUIPMENTS

The test results of the obtained films are shown in Table I. The haze values were measured in accordance with the method of ASTM D1003-95 using a haze meter (TOYO SEIKI). The 60° gloss was measured in accordance with the method of Japanese Industrial Standard K7105 using a digital varied-angle optometer (SUGA SHIKENKI). The surface roughness ***Ra*** was measured by a surface roughness-meter (type SAS-2010; MEISHIN KOKI.).

The final film was image-captured by an optical microscope with 500 times magnification and the captured image was converted to a digital file using an image capture board. Figure 1 shows images of the raw specimens. Three test films [Figure 1(a–c), designated as "F1"–"F3", respectively), which were generated at a different day, were compared with a reference film [Figure 1(d), designated as "L1"]. Each film was image-captured three times. C++ language was used for the programming and the execution time took less than one minute for an image with about a thousand beads at Pentium IV 3.0-GHz dual-core CPU.

THEORY

The procedure for quantifying the positional randomness of beads are composed of mainly three steps of an image processing step (details in Image Analysis section), a triangulation step (in Delaunay Triangulation section) and a dispersity index calculation step (in Modified Version of Static Dispersity Index Calculation section to Stable Relaxation of Bead Positions to a Hexagonal-Packing Form section).

Image Analysis

Firstly, several conventional image processing operators[18] were used to extract and identify the beads from the background (Figure 1). A raw image from a microscope with 1280 × 1024 pixels was used in this investigation. The raw image was histogram-equalized and thresholded to simplify the gray level image into a black/white binary image. Adaptive Gaussian thresholding with window size of 55 × 55 and zero offset value was used. Window size less than 55 did not produce a satisfactory segmentation result.

Then, the binary image was eroded and dilated to eliminate small image noises such as dots. Canny edge finding algorithm was used to find the contours of fibers. This step was a preliminary step for the watershed algorithm,[19] which was used to find closed-loop objects, i.e., bead boundaries, in an image.

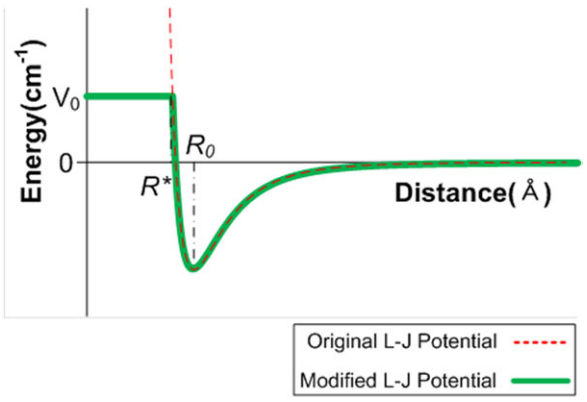

Figure 2. Illustration of the original and modified Lennard-Jones potential. [Color figure can be viewed in the online issue, which is available at wileyonlinelibrary.com.]

Delaunay Triangulation

Before calculating the dispersity index of segmented beads, it would be better to reduce redundant calculations in advance. As our method calculates interactions among beads, a bead pair located very far away does not make a meaningful contribution to the results. Voronoi tessellation,[20] which gives equidistance boundary among neighbor beads, was used to filter out such unnecessary interaction pairs. Two beads are said to be "neighbors" if they share a common edge in a Voronoi diagram. The neighbor pairs were graphically demonstrated by Delaunay triangulation, which is a dual form of Voronoi diagram. Redundant calculations were skipped by considering only the valid bead pairs from the Delaunay triangulation meshing result.

Modified Version of Static Dispersity Index Calculation

We defined the static version of the dispersity index in our previous work.[17] Before advancing to our new relaxation-based dispersity index concept, it is necessary to modify the previous static version for clarifying the effects of bead repulsion/contraction potentials. The basic idea is that beads are virtual molecules, which do not have any motion conceptually in this static version, and that their molecular potentials among neighbor beads represent the positional randomness of the beads. The classical Lennard-Jones (L-J) potential was adopted for the calculation of the virtual interbead potential. The common expression of L-J potential is

$$V_{LJ}(r) = 4\varepsilon_0\left[\left(\frac{\sigma}{r}\right)^{12} - \left(\frac{\sigma}{r}\right)^{6}\right] \quad (1)$$

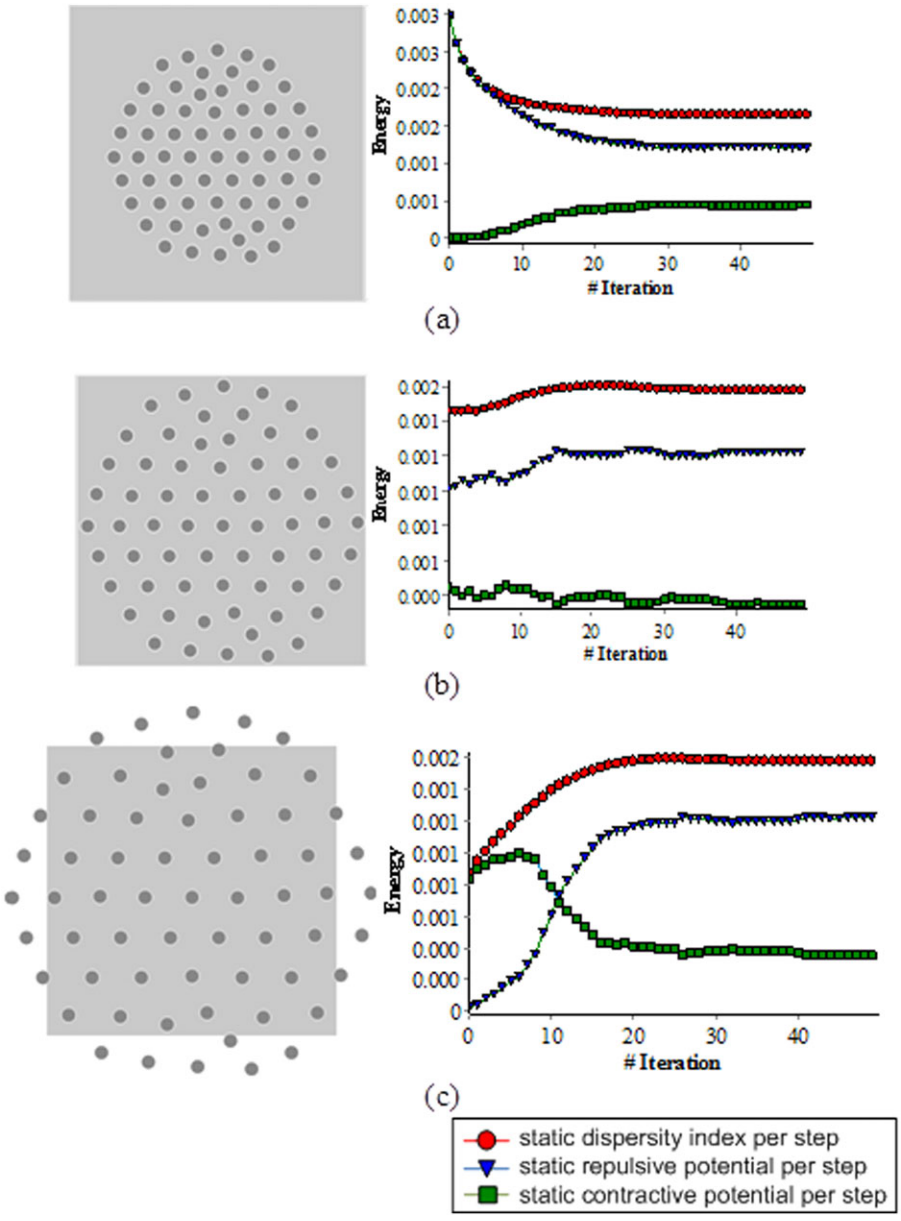

Figure 3. Per-step variation of energy terms comprising static dispersity index (left row: bead image, right row: graph of repulsion/contraction energy and their sum). [Color figure can be viewed in the online issue, which is available at wileyonlinelibrary.com.]

where ε_0 is the depth of the potential well and σ is the distance at which the interparticle potential is zero, and r is the distance between the particles.[21] ε_0 and σ were set to a value of 1 arbitrarily to minimize a floating point round-off error during numerical calculations.

Now we propose a modified version to prevent the potential from diverging to infinity when $\boldsymbol{r}$ is close to zero.

$$V_{\mathrm{mod}}(r) = \begin{cases} V_0 = V_{LJ}(R^*) & (r < R^*) \\ V_{LJ}(r) & (r \geq R^*) \end{cases} \quad (2)$$

where $\boldsymbol{R^*}$ is a threshold that has the same value as an average bead radius in this investigation. Figure 2 illustrates the original and modified L-J potential. The modified potential can be dissected into two regions with respect to the minimum energy distance R_0. The left side is so called the Pauli repulsion region that is dominated by the term $(\sigma/r)^{12}$. This region makes repulsive forces to scatter neighboring beads and we define this force as a repulsion force or a distribution force. The right side is the van der Waals force region that comes from the second term, $(\sigma/r)^6$, which will be defined as a contraction force or a dispersion force. The new version of the static dispersity index is defined as a sum of potentials from both the repulsion force and the contraction force among neighbor beads.

Dynamic Dispersity Index Calculation

The modified static dispersity index was defined in the previous section. Unfortunately, we found that it showed some errors when the number of beads increased. So we defined another concept, dynamic dispersity index for more accurate evaluation. The assumption is that the beads are virtually "moving" gas molecules, which are motivated by the repulsion/contraction forces from L-J potential. The simulation goes on with a suitable time step until there is no energy difference by movement. The dynamic dispersity index is the sum of static dispersity index during all the time steps. Similarly to the static index calculation, the potential from both the repulsion and the contraction were recorded separately to reveal the effects of repulsive force and contractive force.

Stable Relaxation of Bead Positions to a Hexagonal-Packing Form

To realize the above-mentioned dynamic dispersity index calculation, the mesh structure found by Delaunay triangulation, which has some residual strain in its edges due to the L-J potential forces, should be relaxed to an equilibrium state. We designated this process as "relaxation". Fortunately, the beads had almost the same radial size in this investigation. Therefore we set the equilibrium distance ($\boldsymbol{R^*}$) among particles as a constant value, which makes the final equilibrium mesh configuration look like a triangular tiling or a hexagonal-packing form. As we need to integrate the static dispersity index value throughout the relaxation process, the relaxation should go on at a certain time step, h. An efficient and numerically stable integration algorithm is needed for such a dynamic simulation. Explicit methods such as explicit Euler did not converge when the number of particles was large, e.g., more than 1000. Instead, we used the semi-implicit version of the dynamic integration, which originally devised for the stable simulation of a cloth.[22] The governing equation of the semi-implicit method is as follows:

$$(\mathbf{M} - h\frac{\partial \mathbf{f}}{\partial \mathbf{v}} - h^2\frac{\partial \mathbf{f}}{\partial \mathbf{x}})\Delta\mathbf{v} = h\left(\mathbf{f}_0 + h\frac{\partial \mathbf{f}}{\partial \mathbf{x}}\mathbf{v}_0\right), \quad (3)$$

where $\mathbf{M}$ is the $3n \times 3n$ diagonal mass matrix whose diagonal elements are $m_0, m_0, m_0, m_1, m_1, m_1, \ldots, m_{n-1}, m_{n-1}, m_{n-1}$.(m_i is mass of particle i, whereas n is the number of particles or beads). $\mathbf{f}$, $\mathbf{v}$, and $\mathbf{x}$ represent force, velocity, and position vectors of particles, respectively. All we need is to define the force vector $\mathbf{f}$ and its derivative, which is composed of only tension term ($\mathbf{f}^T$) in this case:

$$\mathbf{f}^T = k_T(\|\mathbf{x}_{ij}\| - l_0)\frac{\mathbf{x}_{ij}}{\|\mathbf{x}_{ij}\|} \quad (4)$$

$$\frac{\partial \mathbf{f}^T}{\partial \mathbf{x}_j} = k_T\frac{(\|\mathbf{x}_{ij}\| - l_0)}{\|\mathbf{x}_{ij}\|}\mathbf{I}_{33} + k_T\frac{l_0}{\|\mathbf{x}_{ij}\|}\mathbf{I}_{33}\frac{\mathbf{x}_{ij}\cdot\mathbf{x}_{ij}^T}{\|\mathbf{x}_{ij}\|^2}, \quad \frac{\partial \mathbf{f}^T}{\partial \mathbf{v}_j} = 0 \quad (5)$$

The above tension force ($\mathbf{f}^T$) is the most basic form of the tension force between two particles, which suffices our demand in this investigation. k_T is a spring constant, l_0 is an equilibrium distance ($=\boldsymbol{R^*}$, in this case), and $\mathbf{x}_{ij}$ is the position vector between two particles. The equilibrium length of eq. (4), l_0, was set to a square root of an image area, to normalize the image size effect. Inserting eqs. (4) and (5) makes eq. (3) to be a linear equation. Solving the linear system gives velocity and final positions of the particles in the next time step.

RESULTS AND DISCUSSION

Difficulties in verifying our method lie in that there have been few researches and presumably no standard method on the direct and nondestructive evaluation of the positional randomness of beads. So we chose two ways for verification. The first

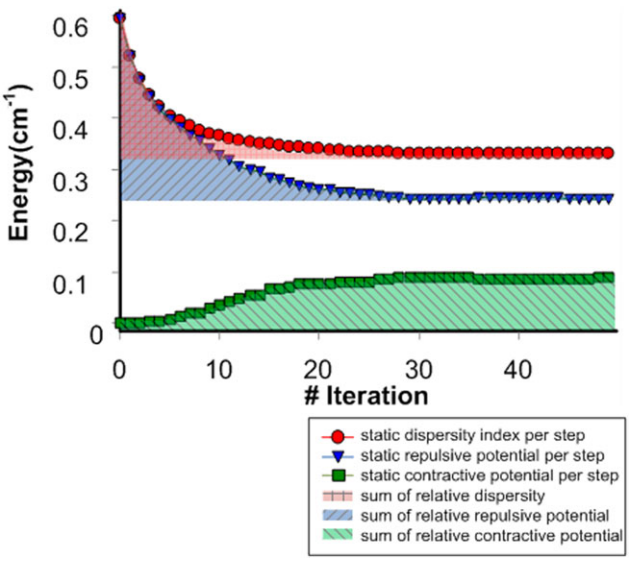

Figure 4. Integration strategy of dynamic dispersity index during relaxation simulation. [Color figure can be viewed in the online issue, which is available at wileyonlinelibrary.com.]

method was comparing the dynamic index with the visual assessment for the graphically drawn sample bead images, which had visually perceptible tendency of the randomness. The second method was comparing the calculated index values with the experimental test method, especially with the haze test, for the real AG film images.

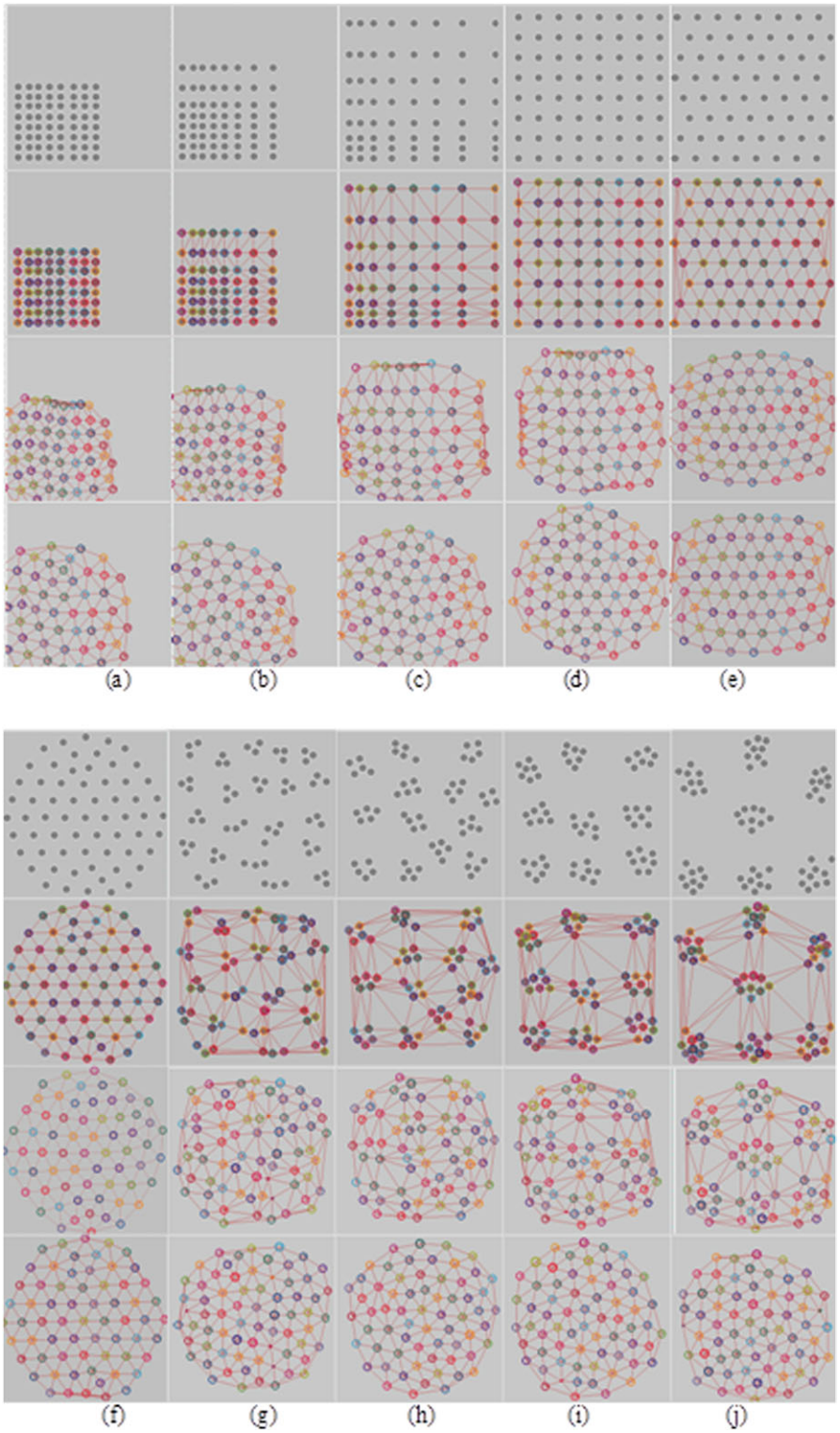

Figure 5. Effect of distribution for bead positional randomness measurement using molecular dynamics analogy (first row: raw data, second row: triangulation results, third row: relaxation progress screen shot, fourth row: final relaxed state, a–d: Scenario II, g–j: Scenario III). [Color figure can be viewed in the online issue, which is available at wileyonlinelibrary.com.]

Applied Polymer SCIENCE

Comparison with Visual Assessment

Before the verification, we need to discuss on the concept of global and local randomness.[17] Practically, beads in real specimens are not perfectly isolated, but make some degree of agglomeration. Positional randomness of particles is determined not only by interparticle neighbor information, but also by the relative size of the particle groups with respect to the boundary image size. We designated the former type (interparticle relationship) as "dispersion" or the "local randomness", and the latter (relative group size) as "distribution" or the "global randomness", based on the concept proposed by Liang and Li.[23] For a polymer composite to have regularly distributed reinforcement particles, the particle groups should be located all over the boundary frame (global randomness) and each local group should have inner particles regularly distributed (local randomness). A reliable evaluation system of the bead dispersity should be able to describe both effects quantitatively.

Figure 3 shows the effect of the distribution and the dispersion for the bead configuration set designated as a scenario I. The three images have the same number of beads and the same neighbor configuration, whereas their relative sizes only differ. The statistical methods of Liu[14] and Diebold[15] could not distinguish such a difference when the number of particles were relatively small.[17] The right-hand-side graphs of Figure 3(a–c) are per-step recordings of the repulsive energy and the contraction energy. Sum of two energy terms are defined as the static dispersity index. Figure 3(b) represents the equilibrium (hexagonally aligned) state of particles, where the tension, compression and their sum do not vary much. The minor fluctuation comes from the virtual Brownian motion of the particles due to the L-J potential because we did not consider any further damping force terms in eq. (4) for the sake of brevity. Figure 3(a) is for the case where the particles are initially compacted, and it shows that the tension force decreases and the compression increases as the simulation goes on. Figure 3(c) is for the other case where the force terms show the opposite tendency. Overall, the net dynamic index, which is the sum of the repulsion and contraction force, shows linear tendency among three images. Previous methods of Liu[14] and Diebold[15] did not consider such a dual-layer effect of the global/local randomness, thus their results were not satisfactory.

Figure 4 shows the integration strategy during the relaxation simulation. The concept of the positional randomness is similar to that of entropy in thermodynamics. Entropy is rather a relative amount of randomness than an absolute value that can be evaluated directly. Likewise, energy terms from the L-J potential was subtracted by the initial step values. Thus, the shaded areas of Figure 4 were used as the true integration results. Without consideration of this "entropy" concept, the final dispersity indices may have erroneous values. For example, the static index of Figure 3(b) maintains a meaningless nonzero value although the beads are in a fully relaxed state.

Now, more sophisticated images were used for verification. Many possible configurations of beads were graphically synthesized to reflect the real cases as shown in Figure 5. Figure 5(a–d) were grouped and designated as a scenario II, which was more general case than the scenario I. Figure 5(e, f) correspond to near-equilibrium and equilibrium states of particles, respectively. Figure 5(g–j) belong to a scenario III, which has 3, 5, 7, and 9 inner beads, respectively, per local group. Their resultant integration values are shown in Figure 6. The scenario II shows linear relationship as is predicted from the results of the scenario I. The scenario I differs from the scenario II in that the beads are not in initial hexagonal packing and their mass of center is not the same. Nevertheless, the dynamic dispersity indices of Figure 6, especially values of a–d, still maintain the linear relationship with the visual assessment. The scenario III is more similar to real AG films than the scenario I or II. Although the scenario III did not have a large number of particles, their tendency was elucidated vividly and matched with the visual assessment.

Figure 6 shows the dispersity measurement for the scenarios II and III of Figure 5. Unlike the apparent tendencies of the dynamic dispersity index, the sum of the relative repulsive/contractive potential, the simple sum of the static dispersity indices or static dispersity index of the initial step without additional relaxation process shows no apparent relationship. This is because the above-mentioned "entropy" effect of randomness is neglected.

Comparison with Haze Test

Finally, the proposed method was applied to the real microscopic images of the AG films of Figure 1. After applying image processing operators, the bead positions were detected. The size variation of the beads was also detected, but specific data were not listed because they had almost the even distribution. Figure 7 shows the results of the image processing operators. Based on the detected bead positions, the tension force and its derivatives of eqs. (4) and (5) were calculated to construct the linear system of eq. (1). Note that the omitted derivatives of eq. (5)

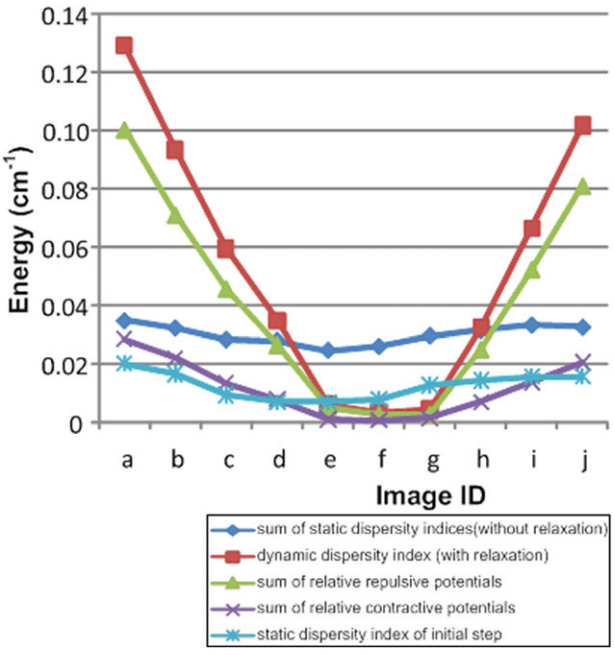

Figure 6. Dispersity index data of Figure 5. [Color figure can be viewed in the online issue, which is available at wileyonlinelibrary.com.]

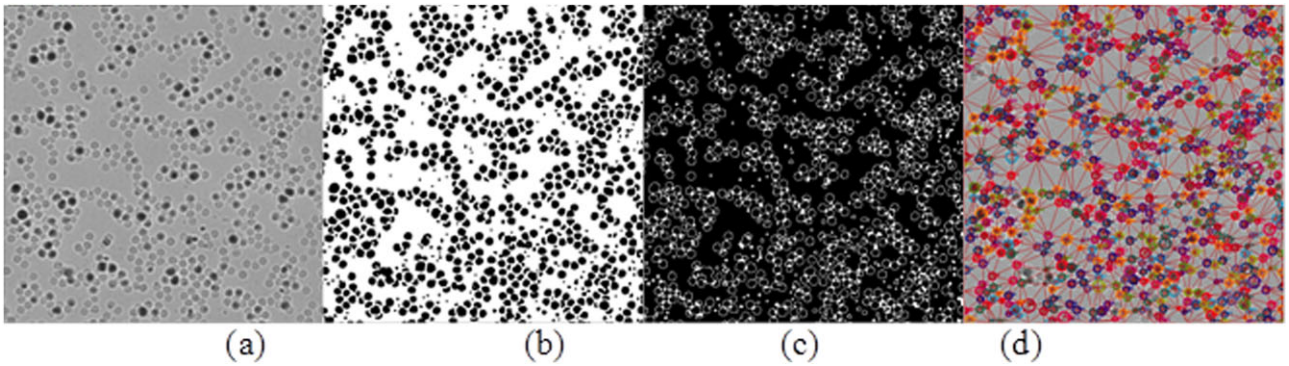

Figure 7. Image processing example of TAC film (a: original image, b: thresholded, c: edge detected, d: watershed and Delaunay triangulated). [Color figure can be viewed in the online issue, which is available at wileyonlinelibrary.com.]

would make eq. (1) to an explicit form, which could result into diversion of the integration. The dynamic dispersity result was compared with the haze test results as shown in Table I and Figure 8. Each haze value was averaged from three repetitions. It is hard to notice visual differences in the bead randomness between the reference and the samples, or among the samples. It is true that the haze test have been the only reliable method that can evaluate the quality objective and numerically until now. The results from the proposed dynamic dispersity index show similar tendency to the haze test result. This signifies that the dynamic dispersity index method can replace the conventional haze test. As this method uses only microscopic image, it is nondestructive and can be done fast, not to mention that it is an objective method, which needs no user intervention. The user does not need to have any background on statistics because the final value is only a single scalar value. Moreover, it can be said to be a direct representation of the bead dispersity because the evaluation is based on the two-dimensional displacement of the beads.

This method can be applied to any other micro- or nano-scale materials where the particles or beads have the same shapes and sizes. The size and the shape are also important factors especially for the particle-shaped materials. But it is quite difficult to analyze the effects of them to the positional randomness. So we leave them as a further work.

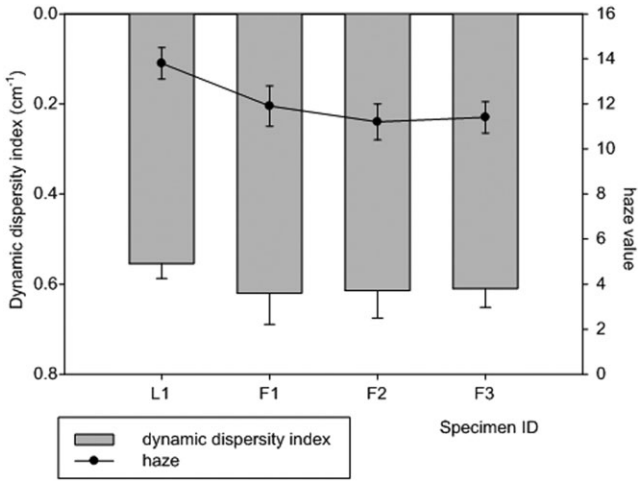

Figure 8. Comparison of dynamic repulsion energy and haze values for TAC films (the lower dispersity index means the better dispersion, the lower haze value means the more transparency).

CONCLUSIONS

This article presents an advanced technique to evaluate the positional randomness of the beads quantitatively. To the best of our knowledge, this is a novel methodology to measure the bead dispersity for the quality control of AG films. The basic assumption is that the film quality is related with the dispersity of silicon beads on the film surface. Microscopic images were captured from the film surface and the bead positions were extracted using image analysis operators. Delaunay triangulation was used to find neighbor information and to reduce redundant calculations. Dynamic dispersity index was calculated by assuming differential energies from pseudo-relaxation process of beads into hexagonal form. The proposed method was verified by comparisons with both visual assessment and haze test. The main contribution of this paper is to provide a direct way of quantifying the dispersity state of AG film beads. The dynamic dispersity index is a simple scalar value, which can be interpreted easily, and the method can be applied to any other positional randomness applications if only they have constant particle shapes and sizes.

REFERENCES

1. Abe, K.; Sanada, Y.; Morimoto, T. *J. Sol Gel Sci. Technol.* **2001**, *22*, 151.
2. Liu, B. T.; Teng, Y. T. *J. Colloid Interface Sci.* **2010**, *350*, 421.
3. Chang, C. C.; Chen, C. M.; Hwang, F. H.; Chen, C. C.; Cheng L.;P. *J. Coating Tech. Res.* **2012**, *9*, 561.
4. Nagahama, T.; Haga, Y.; Matsumura, S.; Suzuki, R. (Sony Corporation), European patent application, EP2 284 580 A1, February 16, **2011**.
5. Tochigi, K.; Tochigi, Y.; Yabuhara, Y. (Topan Printing Co., Ltd.), U.S. patent application 2010/0182551 A1, July 22, **2010**.
6. Kawahara, S.; Takahashi, N. (Nitto Denko Corpoation), U.S. patent 6,970,213 B2, November 29, **2005**.

7. Muramatsu, Y. (Fuji Photo Film Co., Ltd.), U.S. patent application 2006/0092495 A1, May 4, **2006**.
8. Tong, H. S.; Prando, G. (Zenith Electronics Corporation), U.S. patent 5,150,004 A, September 22, **1992**.
9. Liu, B.; Teng, Y.; Lee, R.; Liaw, W.; Hsieh, C. *Colliod Surf. A* **2011**, *389*, 138.
10. Liu, B.; Teng, Y. *J. Colloid Interface Sci.* **2010**, *350*, 421.
11. Shim, J.; Kang, J.; Koo, J.; Chang, Y. U.S. patent application 2012/0321874 A1, December 20, **2012**.
12. Wu, G.; Wang, J.; Shen, J.; Yang, T.; Zhang, Q.; Zhou, B.; Deng, Z.; Bin, F.; Zhou, D.; Zhang F. *J. Non Cryst. Solids* **2000**, *275*, 169.
13. Hiller, J.; Mendelshon, J. D.; Rubner, M. F. *Nature Mater.* **2002**, *1*, 59.
14. Liu, S., In A Guide to Materials Characterization and Chemical Analysis, Wiley_VCH: Danvers, **1996**; Chapter 9.
15. Diebold, M. P. In 8th Nürnberg Congress, Creative Advances in Coatings Technology, Nürnberg, Germany, April 25–28, **2005**.
16. Huckaby, D. K. P.; Caims, D. R. In SID Symposium Digest of Technical Papers, Wiley: Wiltshire, Great Britain, **2009**.
17. Sul, I. H.; Youn, J. R.; Song, Y. S. *Carbon* **2011**, *49*, 1473.
18. Russ, J. C. In The Image Processing Handbook, CRC Press: Florida, **2008**.
19. Vincent, L.; Soille, P. *IEEE Trans. Pattern Anal. Mach. Intell.* **1991**, *13*, 583.
20. Shewchuk, J. R. *Comput. Geom.* **2002**, *22*, 21.
21. Lennard-Jones, J. E. *Proc. R. Soc. A Math. Phys. Eng. Sci.* **1924**, *106*, 463.
22. Baraff, D.; Witkin, A. In Proceedings of Computer Graphics, Annual Conference Series, Orlando, **1998**, p 43.
23. Liang, J. Z.; Li, R. K. Y. *J. Reinf. Plast. Compos.* **2001**, *20*, 630.